Title
Nanoporous gold assemblies of calixarene-phosphine-capped colloids

Journal
Chemical Communications, 53(79)

ISSN
1359-7345

Authors
Schöttle, Christian
Clark, Ezra L
Harker, Audrey
et al.

Publication Date
2017-10-03

DOI
10.1039/c7cc05116f

Peer reviewed

Volume 53 | Number 79 | 11 October 2017 | Pages 10841–10964

ChemComm

Chemical Communications

rsc.li/chemcomm

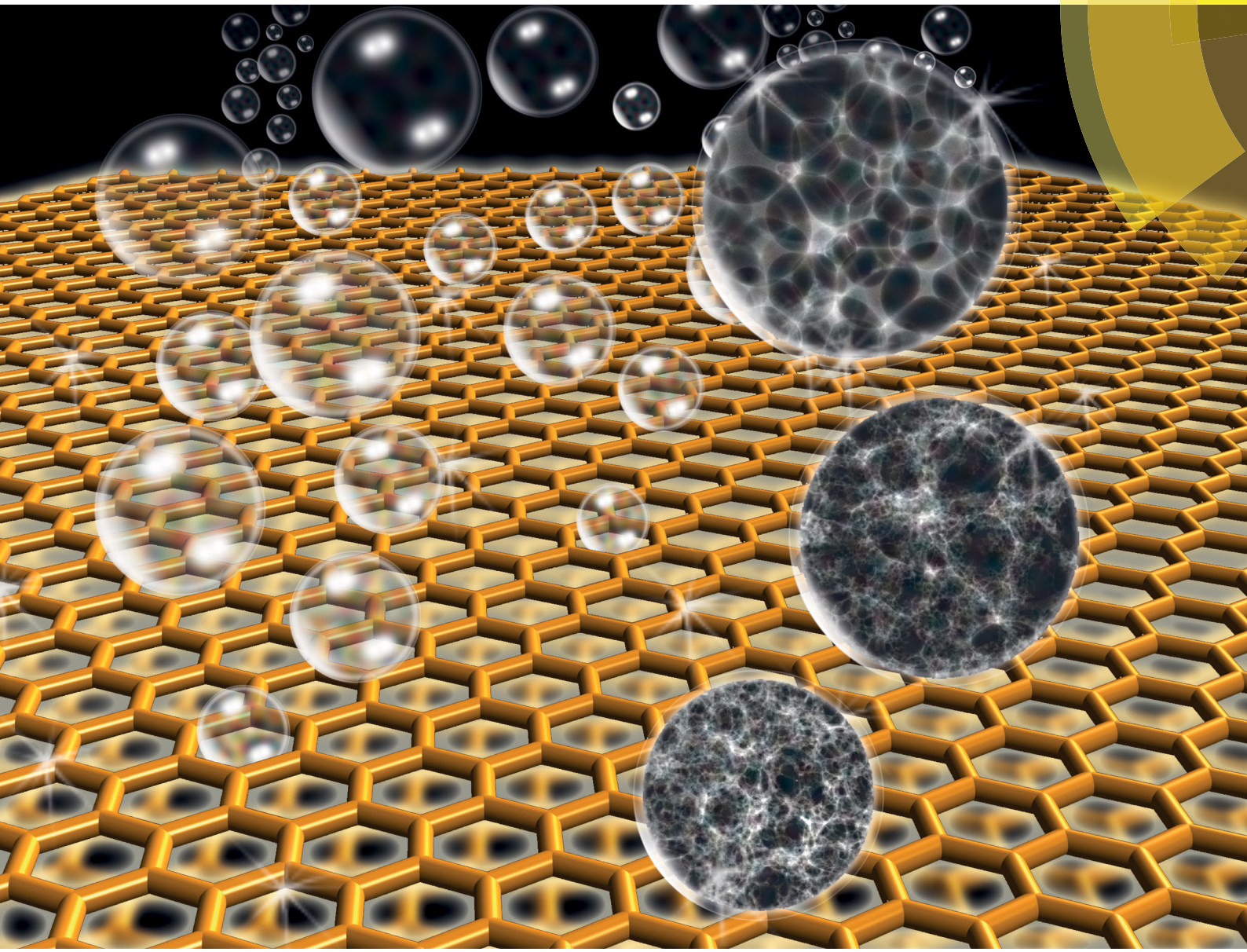

ISSN 1359-7345

ROYAL SOCIETY OF CHEMISTRY

COMMUNICATION

Alexander Katz *et al.*

Nanoporous gold assemblies of calixarene-phosphine-capped colloids

ChemComm

COMMUNICATION

View Article Online
View Journal | View Issue

Cite this: *Chem. Commun.*, 2017, 53, 10870

Received 2nd July 2017,
Accepted 30th August 2017

DOI: 10.1039/c7cc05116f

rsc.li/chemcomm

Nanoporous gold assemblies of calixarene-phosphine-capped colloids†

Christian Schöttle,[a] Ezra L. Clark,[ab] Audrey Harker,[a] Andrew Solovyov,[a] Alexis T. Bell[ab] and Alexander Katz*[a]

The synthesis of high surface-area colloidal assemblies of calixarene-phosphine-capped nanoporous gold is reported under reductive electrochemical conditions. These materials uniquely exhibit a remarkably thin wall thickness down to 10 nm, while possessing pore sizes on the order of up to hundreds of nanometers, which can be controlled *via* choice of organic ligand.

The nanoscale patterning of materials is central to both fundamental science as well as technological applications in areas such as biotechnology and medicine, electronics, optics, sensors and actuators, membranes, catalysis, fuel cells, and energy harvesting and storage.[1–3] There has therefore been great interest in development of synthetic approaches for patterning materials on the nanoscale, which typically involves a template, and a replication process comprising growth of the material to be nanostructured around this template, followed by template removal.[4,5] Here, we demonstrate the synthesis of a patterned material consisting of nanoporous gold, under electrochemically reducing conditions that assemble calixarene-bound gold cluster colloids into a hexagonally ordered and porous configuration, in a manner that is controlled by chelation of the calixarene ligand.

Nanoporous gold has been previously well known as a conductive metal possessing high surface area.[1,5] These materials have typically exhibited wall thicknesses that are approximately the same as their pore size (*i.e.* the aspect ratio defined by the ratio of the pore size to the wall thickness has been approximately unity).[1,5] A unique feature of our nanoporous gold is its high aspect ratio of pore size (*e.g.*, several hundred nanometers) to wall thickness (*e.g.*, 10 nm), which results in a higher exposed metal surface-to-volume ratio for our material – a desirable attribute for the applications described above.

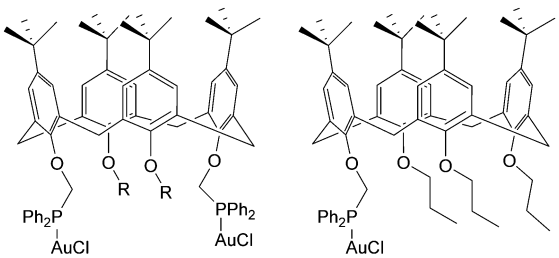

1a: R = Me
2a: R = nPr

3a

Fig. 1 Phosphine-calixarene gold chloride complexes used as precursors for the synthesis of Au clusters **1b**, **2b** and **3b**. The clusters are functionalized with the corresponding calixarene.

Our approach for synthesizing nanoporous gold involves colloidal assembly of calixarene-functionalized gold clusters as building blocks, which are obtained as previously reported, by reduction of calixarene-phosphine gold chloride molecular complexes **1a**, **2a** and **3a** with excess of ethanolic $NaBH_4$, to yield gold clusters **1b**, **2b** and **3b**, respectively.[6] These gold-cluster building blocks consist of a comparative series of ligands (Fig. 1), which are either mono- (**3b**) or bidentate-calixarene-phosphines on the metal surface (sterically crowded narrow rim with propoxy substituents in **2b** and sterically less encumbered narrow rim with methoxy substituents in **1b**), and all exhibit a narrow size distribution below 1.2 nm *via* high-angle annular dark-field scanning transmission electron microscopy (HAADF-STEM) (see Fig. S1–S5 of ESI†).

Drop casting an ethanolic solution of calixarene-stabilized gold cluster building blocks comprising **1b**, **2b** and **3b** on glassy carbon electrodes followed by treatment under electrochemical conditions at a fixed potential of −1.5 V *vs.* reversible hydrogen electrode (RHE) using a carbon-dioxide saturated solution of aqueous cesium carbonate as electrolyte results in the transformation of gold clusters **1b**, **2b**, and **3b** to corresponding porous colloidal metal–organic assemblies **1**, **2**, and **3**, respectively, on the electrode surface. During this process, a slight

[a] *Department of Chemical and Biomolecular Engineering, University of California at Berkeley, Berkeley, California 94720, USA. E-mail: askatz@berkeley.edu*
[b] *Joint Center for Artificial Photosynthesis, Lawrence Berkeley National Laboratory, Berkeley, California 94720, USA*

† Electronic supplementary information (ESI) available: Experimental details, additional figures. See DOI: 10.1039/c7cc05116f

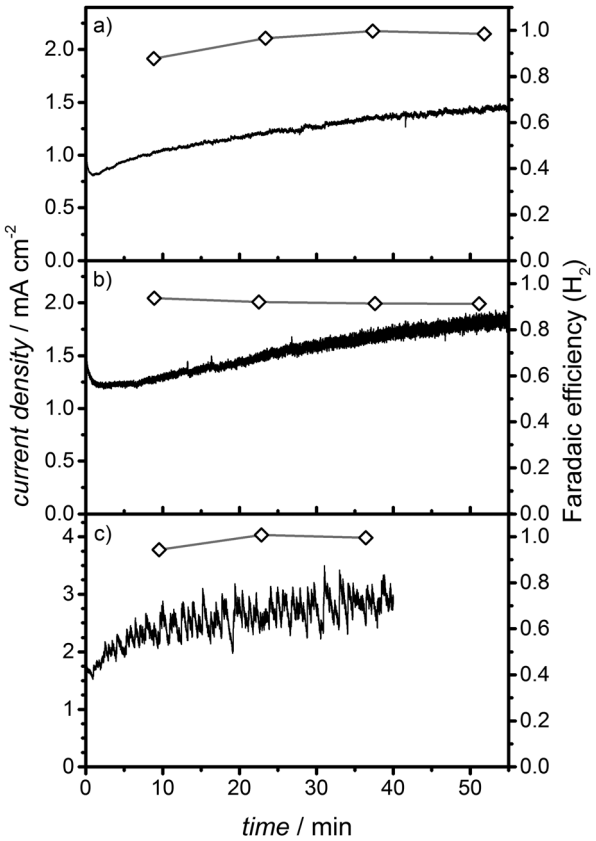

Fig. 2 Current density and Faradaic efficiency of H_2 formation of **1** (a), **2** (b) and **3** (c) at a fixed potential of 1.5 V *vs.* RHE. Solid line represents current density, whereas diamond symbols represent H_2 Faradaic efficiency.

increase in the current density over time was observed, before a plateau starting at 40–50 minutes in Fig. 2. H_2 is formed with a Faradaic efficiency of 90–95% when using **1b**, **2b**, and **3b** as building blocks, shown in Fig. 2. This high H_2 Faradaic efficiency and the observed nearly complete absence of products resulting from CO_2 reduction (*e.g.*, CO) of less than 1% (analyzed *via* gas chromatography of gas stream flowing through electrochemical cell) is consistent with expectations based on prior studies,[7] given the small size of our gold-cluster building blocks and the expected prevalence of gold atoms of low coordination comprising them (*vide infra*).[6]

The resulting nanoporous gold assemblies **1**, **2**, and **3** were characterized *via* HAADF-STEM in Fig. 3 (see Fig. S7–S9, ESI†). These assemblies consist of pore sizes on the order of hundreds of nanometers and nanoscale wall thicknesses ranging down to about 10 nm in **1** and **2**, while being larger in **3**. The wall thickness in **3** appears to be inhomogeneous with thicker areas acting as connectors to thinner wall sections that are characteristic of the thickness observed in **1** and **2**. While **2** also exhibits inhomogeneity, the size of the thicker areas in this sample is significantly smaller than observed in **3** and more similar to its wall thickness of 10 nm. Images at higher magnification in Fig. 4b, d and f show that the pore walls of these porous structures consist of a granularity on the length scale of slightly less than 1.2 nm, suggesting the pore wall is comprised of partially coalesced gold-cluster building blocks, the same ones used for materials synthesis. Consistent with this, the UV-Vis spectrum of **1** exhibits no surface plasmon absorption, which would otherwise have been expected for larger gold nanoparticles (see Fig. S6, ESI†). Only a shoulder at 400–450 nm is visible, which appears more prominently but in the same wavelength range as a distinguishing plateau band in the gold-cluster building block **1b**, having been previously assigned to the absorption band of a Au_{11}-sized cluster.[8]

A comparison of the different calixarene-phosphine ligands can be conducted based on data in Fig. 3. The bidentate calixarene-phosphine ligands in **1** and **2** lead to the smallest pores and highest surface-area materials, while the monodentate ligand in **3** exhibits the largest pore sizes. These HAADF-STEM results are supported by electrochemical measurements of the relative specific surface area, which we expect to vary inversely with the wall thickness. These electrochemically measured relative areas are similar when using a bidentate ligand in **1** and **2**, but are 3-fold lower for the monodentate ligand in **3** (see Table S1 in ESI†). We thus observe a clear trend that the wall thickness of the resulting nanoporous gold colloidal assembly decreases in Fig. 3, as the degree of interaction between gold surface and ligand increases (*i.e.* as a result of bidentate bonding). We also observe a correlation between the wall thickness and the pore size, wherein thicker walls in **3** support a larger pore size compared to **1** and **2**. These data unequivocally demonstrate the role of the calixarene-phosphine ligand in controlling the nanoscale morphology of the resulting materials.

The relatively high content of organic ligands in these materials leads to significant observed beam damage in the electron beam, which forms amorphous carbon during HAADF-STEM experiments (Fig. S10, ESI†). Crucially, the beam damage of the organic ligands leads neither to a collapse nor a change of the porous structure. Nanoporous gold materials **1**, **2**, and **3** are highly dispersible in organic solvents such as dichloromethane. We posit that this solubility may be enhanced by the organic calixarene functionalization of the colloidal assembly comprising the nanoporous gold after electrochemical synthesis. Repetitive dissolution and drying of the materials leads to no change in morphology *via* HAADF-STEM. In contrast, as a comparative control, a gold cluster without stabilizing calixarene-phosphine ligands (*e.g.*, conventional dodecanthiol-capped Au cluster[9]) synthesized under similar conditions is observed to aggregate and form large, unstructured, sintered dendrites in Fig. 3g and h.[10] Based on our ability to disperse and redeposit **1**–**3** on various substrates, we surmise intercluster gold–gold bonding in these materials. This gold–gold bonding between clusters must be sufficient so as to retain a stable and unaltered nanoporous gold network during both drying of organic solvent and ligand removal (*vide supra*). It differentiates our materials from those previously synthesized using breath-figure templating of gold nanoparticles,[11,12] in which there does not appear to be bonding between gold nanoparticles (*i.e.* distinct 3 nm nanoparticles comprise the assembly pore wall).[12] Nor is there an ability to disperse and redeposit that assembly after its synthesis, as we do here.

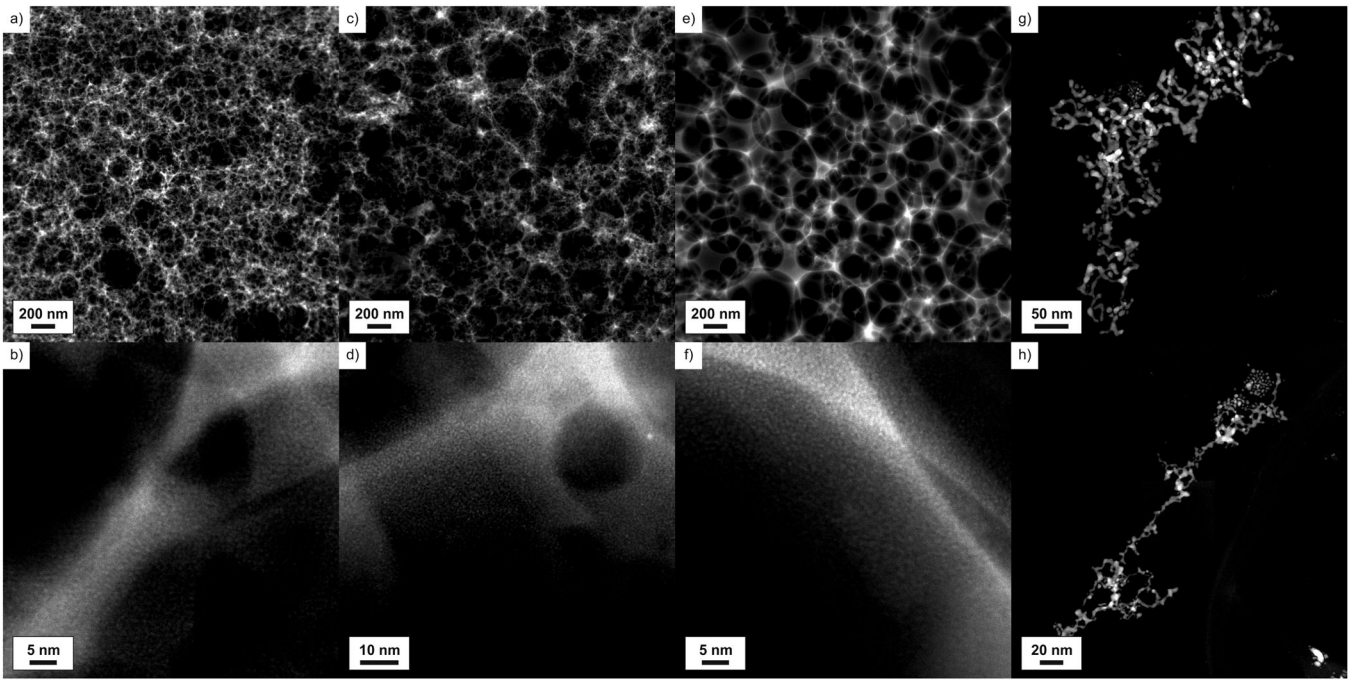

Fig. 3 HAADF-STEM images of the metal–organic porous colloidal assemblies: (a) overview image of **1**, (b) detail image of **1**, (c) overview image of **2**, (d) detail image of **2**, (e) overview image of **3**, (f) detail image of **3**, (g and h) overview images of dodecanthiol-capped Au nanoparticles after applying the same reductive electrochemical conditions.

We performed scanning electron microscopy (SEM) of **2** (representative small-pore material) and **3** (representative large-pore material). The images demonstrate nanoporous gold films that span more than 50 μm for both samples. Larger pores than those observed *via* HAADF-STEM in Fig. 3 become visible on the length scales of the SEM images. For **2**, pores on the size of 1 μm are readily apparent throughout the sample, whereas in **3**, there are numerous even larger pores of up 3 μm evident *via* SEM (Fig. S11 and S12 in ESI†).

Based on all of the data acquired, we hypothesize the following mechanism for formation of the nanoporous colloidal assemblies **1–3**. The basic physical chemistry behind their formation follows that articulated by Hildebrand,[13] which is also based on observations of Pickering,[14] and Ramsden,[15] spanning a century of research into solid colloidal-particle stabilization of oil/water interfaces. More recently, similar phenomena have been captured by the elegant work of Korgel and coworkers,[11,12] when describing the breath-figure templating of gold nanoparticles by water droplets, which are formed upon condensation in an organic fluorocarbon medium (which evaporates during the kinetic templating process). In our case, we invoke H_2 bubbles as the equivalent of an oil phase in a conventional oil droplet in water microemulsion. Akin to water bubbles in breath-figure templating,[11,12] we hypothesize the H_2 bubbles act as templates. In such a mechanism, the hydrophobic calixarene-capped gold clusters in **1–3** assemble at the bubble surface much like a surfactant molecule assembles at either the oil/water or air/water interface.[13] These H_2 bubbles evolve at the gold-cluster catalyst surface *via* water electrolysis, as described by data in Fig. 2. Water desolvates the hydrophobic upper-rim cavity of the calixarene ligands, as it thermodynamically prefers to interact with other water molecules. The H_2 bubble removes the otherwise prohibitive penalty of forming a void that becomes lined with the hydrophobic upper-rim of the calixarene ligands, in this process. We previously characterized the hydrophobicity of these upper rims, and their limited solvation by liquid water.[16] Another process occurring at the same time is formation of intercluster gold–gold bonds. We surmise that the sterically bulky phosphine-calixarene ligands prevent uncontrollable sintering of gold cluster building blocks *via* coalescence to larger nanoparticulate structures, instead directing the formation of a composite metal–organic assembly comprising individual gold clusters possessing limited gold intercluster connectivity. Again, we emphasize that in the absence of calixarene ligands, much more dense aggregates (*i.e.* lacking nanoscale porosity) of gold are obtained as shown by the control in Fig. 3g and h. These dense aggregates are similar in length scale to those reported previously in hydrogen-bubble templated nanoporous gold,[17–19] and, crucially, lack the patterned nanoscale porosity and thin wall thickness of the materials derived from calixarene-ligand-containing building blocks in Fig. 3a–f. The dynamics of H_2 bubble formation, metal–metal bond formation between clusters, cluster diffusivity, and growing H_2 bubble mobility all likely factor into the nanoporous gold-assembly synthesis process. These are to be investigated further in future work.

In conclusion, we demonstrate the synthesis of high specific surface area nanoporous gold, which has been synthesized from three different mono- and bidentate-calixarene-phosphine capped gold-cluster building blocks *via* hydrogen-bubble templating under electrochemically reducing conditions. These organized colloidal assemblies comprise intercluster gold–gold bonds,

which are stable to repetitive solvent evaporation and have pore sizes spanning from tens of nanometers to microns. The size of these pores appears to depend sensitively on the wall thickness and organic surface-ligand employed. We observe thin wall thicknesses, down to the order of 10 nm, in these materials. To the best of our knowledge, this represents the largest aspect ratio consisting of pore-size-to-wall-thickness reported to-date for nanoporous gold, as well as the smallest wall thickness (previously 30 nm). These colloidal assemblies can be used themselves as scaffolds onto which other metals including single metal atoms can be electrochemically deposited for catalysis,[1b,20] among other applications. Due to their open structure and inexpensive one-step synthesis, we envision widespread application in areas already established for similarly nanoporous materials, which possess lower specific surface areas. In particular, the large pore sizes in our materials should facilitate the immobilization of enzymes and other biomolecules.

The authors are grateful to W. Osowiecki (UC Berkeley) for help with the electrode preparation, and to N. Azgui and P. Lum (qb3, UC Berkeley) for SEM imaging. Work at the Molecular Foundry was supported by the Office of Science, Basic Energy Sciences, of the U. S. Department of Energy under Contract No. DE-AC02-05CH11231. C. S. acknowledges Deutsche Forschungsgemeinschaft (DFG) for a research fellowship, and A. K. and C. S. are grateful to the Office of Science, Basic Energy Sciences, of the U. S. Department of Energy under Contract No. DE-FG02-05ER15696 for research funding.

Conflicts of interest

There are no conflicts to declare.

Notes and references

1 (*a*) A. Wittstock, J. Biener and M. Baumer, *Phys. Chem. Chem. Phys.*, 2010, **12**, 12919–12930; (*b*) A. Wittstock and M. Baumer, *Acc. Chem. Res.*, 2014, **47**, 731–739; (*c*) J. Biener, M. M. Biener, R. J. Madix and C. M. Friend, *ACS Catal.*, 2015, **5**, 6263–6270.
2 M. Hernández-Guerrero and M. H. Stenzel, *Polym. Chem.*, 2012, **3**, 563–577.
3 U. H. F. Bunz, *Adv. Mater.*, 2006, **18**, 973–989.
4 X. Y. Yang, L. H. Chen, Y. Li, J. C. Rooke, C. Sanchez and B. L. Su, *Chem. Soc. Rev.*, 2017, **46**, 481–558.
5 O. D. Velev, P. M. Tessier, A. M. Lenhoff and E. W. Kaler, *Nature*, 1999, **401**, 548.
6 N. de Silva, J. M. Ha, A. Solovyov, M. M. Nigra, I. Ogino, S. W. Yeh, K. A. Durkin and A. Katz, *Nat. Chem.*, 2010, **2**, 1062–1068.
7 W. Zhu, R. Michalsky, O. Metin, H. Lv, S. Guo, C. J. Wright, X. Sun, A. A. Peterson and S. Sun, *J. Am. Chem. Soc.*, 2013, **135**, 16833–16836.
8 L. C. McKenzie, T. O. Zaikova and J. E. Hutchison, *J. Am. Chem. Soc.*, 2014, **136**, 13426–13435.
9 M. J. Hostetler, J. E. Wingate, C.-J. Zhong, J. E. Harris, R. W. Vachet, M. R. Clark, J. D. Londono, S. J. Green, J. J. Stokes, G. D. Wignall, G. L. Glish, M. D. Porter, N. D. Evans and R. W. Murray, *Langmuir*, 1998, **14**, 17–30.
10 K. Manthiram, Y. Surendranath and A. P. Alivisatos, *J. Am. Chem. Soc.*, 2014, **136**, 7237–7240.
11 P. S. Shah, M. B. Sigman, C. A. Stowell, K. T. Lim, K. P. Johnston and B. A. Korgel, *Adv. Mater.*, 2003, **15**, 971–974.
12 A. E. Saunders, P. S. Shah, M. B. Sigman, T. Hanrath, H. S. Hwang, K. T. Lim, K. P. Johnston and B. A. Korgel, *Nano Lett.*, 2004, **4**, 1943–1948.
13 P. Finkle, H. D. Draper and J. H. Hildebrand, *J. Am. Chem. Soc.*, 1923, **45**, 2780–2788.
14 S. U. Pickering, *J. Chem. Soc.*, 1907, **91**, 2001–2021.
15 W. Ramsden, *Proc. R. Soc. London*, 1903, **72**, 156–164.
16 J. M. Notestein, A. Katz and E. Iglesia, *Langmuir*, 2006, **22**, 4004–4014.
17 S. Cherevko and C.-H. Chung, *Electrochem. Commun.*, 2011, **13**, 16–19.
18 H. du Toit and M. Di Lorenzo, *Sens. Actuators, B*, 2014, **192**, 725–729.
19 H. du Toit and M. Di Lorenzo, *Biosens. Bioelectron.*, 2015, **69**, 199–205.
20 J. C. Fierro-Gonzalez, J. Guzman and B. C. Gates, *Top. Catal.*, 2007, **44**, 103–114.